Breakthrough Carbon Nanotube–Silicon Heterojunction Solar Cells

Daniel D. Tune,* Nitin Mallik, Heike Fornasier, and Benjamin S. Flavel*

The latest advances in carbon nanotube–silicon heterojunction solar cells are combined with a new doping protocol based on the outstanding electron withdrawing properties and excellent silicon surface passivation ability of sulfonated polytetrafluoroethylene (Nafion). Using this new dopant for carbon nanotube–silicon solar cells, advanced substrate design, and an optimized antireflective texture fast etch with organic base, breakthrough performance is obtained from research grade devices with active areas of 1 and 5 cm^2, which yield power conversion efficiencies of 17.2 and 15.5%, respectively.

Heterojunctions of carbon nanomaterials interfaced with silicon respond to light illumination and can be operated in the power regime as solar cells.[1] As the global photovoltaics industry strives to reduce the levelized cost of electricity through increases in power output and/or reductions in manufacturing costs, this type of solar cell offers potential benefits due to its solution processability, the lack of high temperature diffusion and firing steps, and lower material cost when carbon nanotube wires are used in place of silver metallization. Since the earliest reports of carbon nanotube–silicon solar cells around 2007/08,[2] there has been steady progress in device development focused primarily on aspects relating to

the properties of the nanotube film,[3] or the silicon surface,[4] as well as in understanding of the underlying operational principles.[5] Although relatively good power conversion efficiency of 17% has previously been reported with this architecture, it came from devices with less than 1 mm^2 active areas.[6] Typical efficiencies and active areas reported in recent years have been on the order of 13–16% for ≈9 mm^2,[7] but as the active area has increased into the range of 1 cm^2 or more, the reported efficiencies have tended more toward 10–12% largely due to resistive power losses in the thin nanotube film.[8] Various nanotube dopants and doping schemes have been introduced, such as nitric acid,[9] metal salts,[5c,7c] and metallocenes,[10] as well as a host of interlayers[11] and antireflection/encapsulant coatings.[6,7,12] Of the dopants that have been reported, only the Cu(I)/Cu(II) redox couple reported by Cui et al.[7b] has demonstrated long term stability (up to one year in ambient). Although random pyramid antireflective texturing is a key process throughout silicon photovoltaics, only two previous reports have used it conjunction with nanotube films.[13]

The use of the perfluorinated polymeric acid Nafion has been reported as a stable p-type dopant for carrier selective carbon nanotube films in organic solar cells by Jeon et al. in 2018,[14] and its excellent passivation properties on n-type silicon have been separately detailed by Chen et al.[15] Furthermore, the use of thin polymer films as refractive index matching and/ or interference-based antireflection layers has been reported for the nanotube–silicon architecture.[12,16] However, through the results of new investigations into the use of Nafion in state of the art carbon nanotube–silicon heterojunction solar cells, developed in response to a recent review of advances in the field,[1d] this Communication reports the ability to combine all of these properties within the carbon nanotube–silicon architecture and further compares the performance of devices made using this material to the copper colloid doping method. Using the new doping regime, rationally designed contact finger geometry, combined single-walled/double-walled nanotube film, and an optimized tetramethyl ammonium hydroxide based random pyramid texture etch, record efficiency for the field is achieved over previously unsurpassed active areas.

To begin, high quality, moderately doped, n-type Cz silicon wafers (0.1–0.3 Ω cm, SSP, <100>, 380 μm thickness) with a 100 nm thermal oxide were used, then a two-step UV lithography process and Cr/Au evaporation was applied to form the structure shown in **Figure 1** (with additional photographs in Figure S1, Supporting Information). In the first lithography

Dr. D. D. Tune, Dr. B. S. Flavel
Institute of Nanotechnology
Karlsruhe Institute of Technology
Hermann-von-Helmholtz-Platz 1, 76344 Eggenstein-Leopoldshafen
Germany
E-mail: daniel.tune@isc-konstanz.de; benjamin.flavel@kit.edu
Dr. D. D. Tune
International Solar Energy Research Center Konstanz
Rudolf-Diesel-Straße 15, 78464 Konstanz, Germany
N. Mallik
College of Science and Technology
University of Bordeaux
351 cours de la Libèration, 33405 Talence CEDEX, France
H. Fornasier
Institute of Microstructure Technology
Karlsruhe Institute of Technology
Hermann-von-Helmholtz-Platz 1, 76344 Eggenstein-Leopoldshafen,
Germany

The ORCID identification number(s) for the author(s) of this article can be found under https://doi.org/10.1002/aenm.201903261.

**ADVANCED
SCIENCE NEWS**
www.advancedsciencenews.com
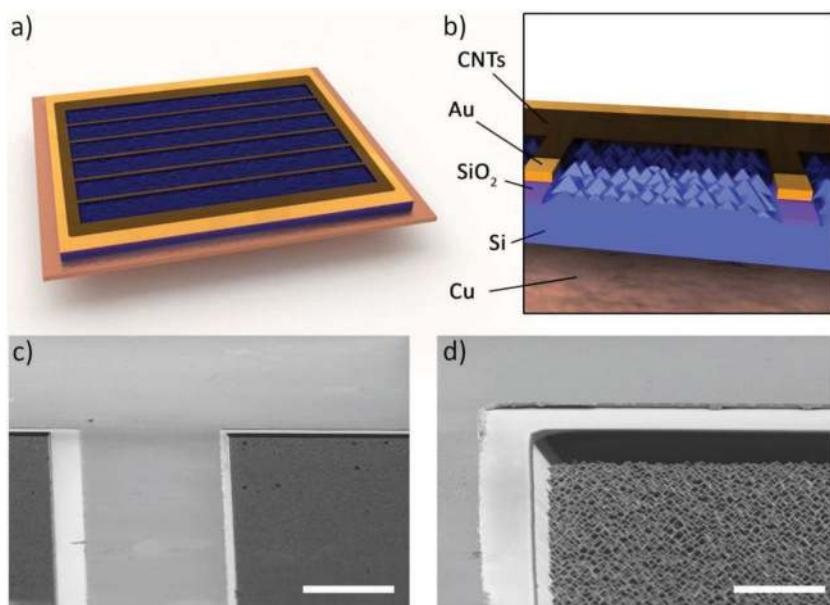
**ADVANCED
ENERGY
MATERIALS**
www.advenergymat.de

Figure 1. a) Graphic representation of device, b) cut out schematic showing the different layers of the device structure, c) electron microscopy image showing the end of a gold contact finger where it joins the rest of the gold electrode that frames the active area, d) higher magnification of the region indicated in (c), showing the gold front electrode and contact finger sitting on SiO$_2$ that has been undercut during the etching of the pyramid texture. Scale bars are 40 and 5 µm in (c) and (d), respectively.

step, the photoresist was used as an HF etch mask to create what would later be the nanotube–silicon junction region. In the second lithography step, the resist was used to define the front side metallization, which was offset from the junction region by 5 µm. This two-step process means that the metallization was not used as the HF etch mask as in many previous reports, and thus prevented the undercutting of the front metallization that occurs during the oxide etch process, as well as during our subsequent texture etch. Additionally, by creating such a stepped structure between the front side metallization and the nanotube–silicon junction area, we reduced the maximum vertical distance over which the nanotube film must stretch (by splitting the total distance into two smaller steps), and produced an overall more robust substrate for research; allowing devices to be exposed to repeated doping, washing, and etching steps without critical failure. The optimum width and pitch of the contact fingers for each substrate size was determined by modelling resistive losses and optical shading,[17] allowing scale up to centimeter-sized devices while maintaining high efficiency (photographs of the substrates shown in Figure S1, Supporting Information). We note that in all later current density calculations, the area covered by the contact fingers was included in the active area. Thus, for a 1 cm^2 device with nine contact fingers of 50 µm width, 4.5 mm^2 was covered by the contact fingers, giving an optical shading of 4.5%. The oxide on the rear sides of the solar cell substrates was etched in a pattern consisting of a regular array of circles in the style of the laser contact opening (LCO) used in some industrial cells to reduce rear side recombination by reducing the contact area, for the same reason. The rear contact fraction was 7.6% and the pattern can be seen in Figure S1 (Supporting Information).

Next, a random pyramid texture was introduced in the junction region as shown in **Figure 2**a and Figure S2 (Supporting Information) by etching in 1% TMAH @ 75 °C for 9 min, resulting in a total reflectance of ≈11% @ 800 nm (Figure 2c,d), but after which further etching did not decrease the reflectance, as shown in Figure S3 (Supporting Information). For the nanotube film, we used a mixture of long double-walled nanotubes and short, small diameter, single-walled nanotubes rich in the semiconducting (6,5) chiral species, that we have developed and optimized for high conductivity, high transmittance, and good dopant response (Figure S4, Supporting Information). The nanotube films were cast from a superacid dope as described previously[4f,5c,e,18] and then floated onto water before being picked up directly onto the target substrates. This yielded surfaces such as that shown in Figure 2b, with the thin nanotube films draped over the pyramids, contacting the upper ≈1/3 of the pyramids' sides and stretching between them. After deposition of the nanotube films the total reflectance was decreased further by ≈1.5% @ 800 nm, most likely due to absorption by the nanotubes, which had transmittances of ≈97.5% @ 800 nm when measured on flat glass (Figure S5, Supporting Information). However, as seen in Figure S5 (Supporting Information), the nanotubes absorbed more strongly in the UV region and less strongly in the IR region, resulting in larger and smaller changes of the reflectance, respectively.

To dope the nanotube films, a colloidal solution of CuCl$_2$/Cu(OH)$_2$ in ethanol/water was first spin coated onto the nanotube–silicon surfaces as per Cui et al.[7b] However, unlike in the case of planar devices, in which the copper colloid effectively reduces reflectance by a combination of scattering, thin film interference effects, and better refractive index matching with air compared to silicon, in this case the surface that resulted after spin coating was somewhat more reflective than before, as shown in Figure 2c. The cause of this can be identified in Figure 2e, where large crystallites of the copper complex can be seen in the nanotube film. It can be surmised that, since the copper complex is not in contact with the silicon surface, it does not provide the improved light coupling into the silicon as on planar devices, and the crystallites instead act as effective back scattering centers. The effect could be clearly observed with the naked eye as a "sparkly" appearance.

However, in contrast to the copper colloid, Nafion can function as a texture-compatible dopant for the nanotube films. Figure 2d shows the pronounced reduction in reflectance that resulted from spin coating of the polymer onto the nanotube-textured silicon surface, with 60–70% decreases across all spectral regions up to around 1100 nm, yielding surfaces with a markedly different appearance to those from the copper colloid (Figure S1, Supporting Information). As seen in Figure 2f, the polymer formed a much more conformal coating on the surface, as expected, but also had the effect of dragging down the
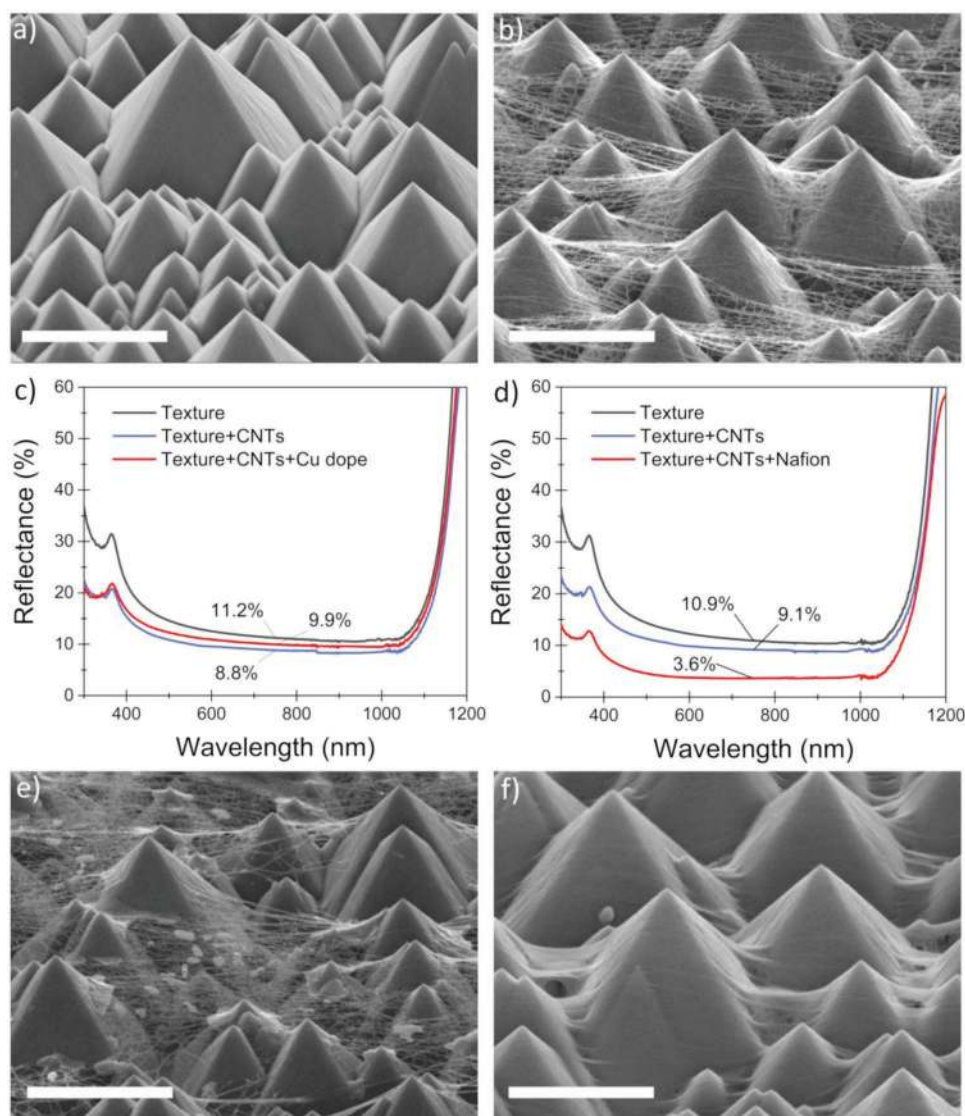
ADVANCED
SCIENCE NEWS
www.advancedsciencenews.com

ADVANCED
ENERGY
MATERIALS
www.advenergymat.de

Figure 2. a) SEM microscopy image showing random pyramid texture formed by TMAH etching, b) optimized carbon nanotube thin film deposited on textured surface, c) reflectance changes with addition of CuCl$_2$/Cu(OH)$_2$ colloidal dopant, d) reflectance changes with addition of Nafion polymeric acid dopant, e) textured surface with nanotube film and colloidal dopant, f) textured film with nanotube film and polymeric dopant. Scale bars are 2 µm.

regions of the nanotube film that had been suspended between pyramids, resulting in a clear increase in the contact fraction between nanotubes and silicon.

Turning now to the solar cell performance, **Figure 3**a shows the IV characteristics of devices immediately after doping with either copper colloid or Nafion polymer. In the case of the copper dopant, the best performing device produced a current density J_{SC} of 28.7 mA cm^{-2}, an open circuit voltage V_{OC} of 611 mV, and a fill factor (FF) of 72.7, yielding a conversion efficiency of 12.8%. The J_{SC} was somewhat lower than previous reports that used the copper colloid dopant, which we attribute to the relatively poor antireflection properties of textured surfaces with this material, while V_{OC} was ≈20 mV higher, which we attribute partly to the higher dopant concentration in the silicon bulk, as well as to the reduced rear side recombination provided by the LCO style patterning, which presumably also

contributed to the relatively high fill factor. As expected based on the reflectance data, the Nafion doped solar cells performed significantly better, with the best device producing a J_{SC} of 32.77 mA cm^{-2}, an outstanding V_{OC} of 661 mV, and an excellent fill factor of 79.0, yielding an efficiency of 17.2%, which is a significant advance in the field when considering the 1 cm^2 active area. In addition to the higher current compared to the copper doped devices, which is due to the lower reflectance of those doped with Nafion, we attribute the high V_{OC} and FF to a combination of excellent surface passivation by the polymer as previously shown by Chen et al.,[15] minimal resistive losses in the optimized front finger geometry, the high quality and moderately high dopant concentration of the bulk, and the low recombination at the patterned rear contact. The quantum efficiency of solar cells with the two types of dopants is shown in Figure 3b,c, and highlights the differences in spectral response.
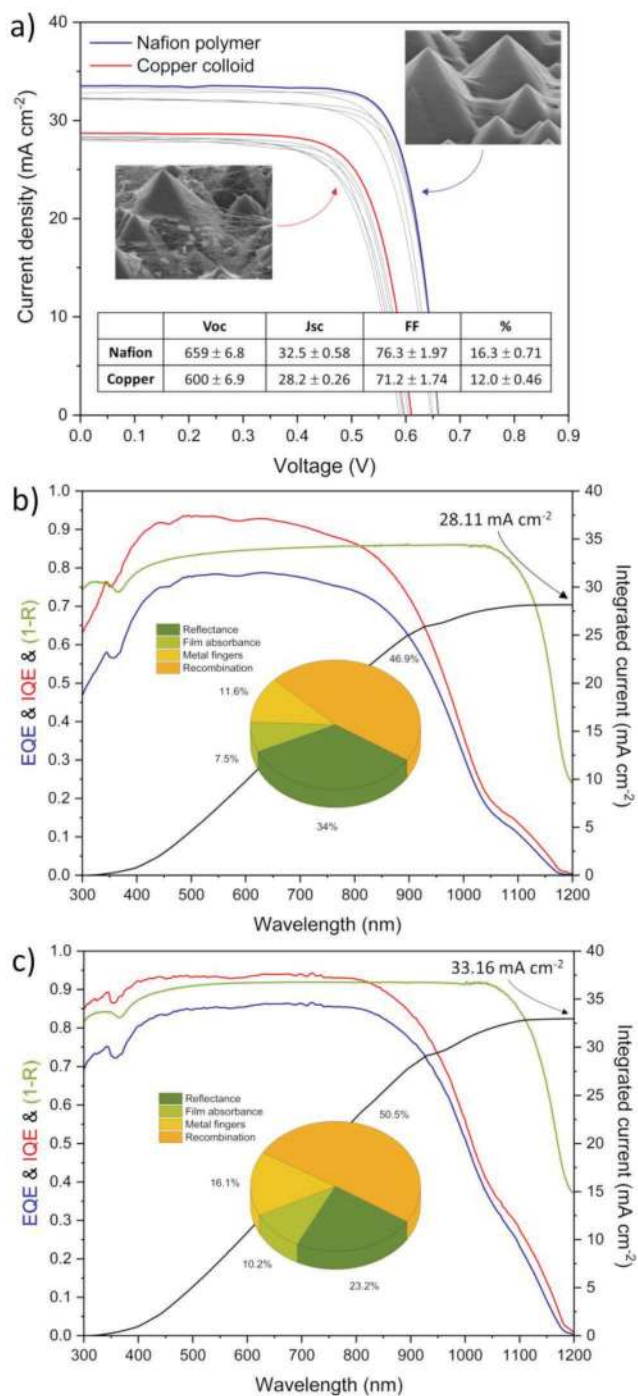
Figure 3. a) Performance of solar cells doped with either copper colloid or polymeric acid, the colored traces are the highest performing devices, median values are given the table, b) quantum efficiency of copper colloid doped devices, c) quantum efficiency of polymeric acid doped devices. The insets of (b) and (c) show the relative contributions to losses due to reflectance, nanotube film absorbance, shadowing by the front side metallization, and recombination.

The copper doped solar cells had a relatively lower QE of maximum 78% due to the higher reflectance, and a clearly lower UV and NIR response. In comparison, the Nafion doped devices had a higher QE of maximum 86% due to the lower reflectance,

and flatter profile due the excellent passivation properties of the polymer. In both cases, the NIR response was improved by the patterned rear contact (Figure S6, Supporting Information). Also in both cases, the internal QE after correcting for reflectance from the surface and the contact fingers was quite good (and was even better when correcting also for the absorbance of the nanotube film, Figure S7, Supporting Information). We attribute this to the fact that in the carbon nanotube–silicon architecture the "emitter" is formed electrostatically by both the difference in Fermi energies of the p-type nanotubes and the n-type silicon, as well as by the fact that the entire charge density in the nanotube film is confined to a region of only a few nanometers in thickness, creating an extremely large and abrupt change in the electric field at the surface. This means that there is none of the Auger recombination due to ionized impurities that is present in solar cells with traditional diffused front emitters. However, the response of the solar cells in the NIR above ≈800–900 nm was poor, predominantly due to the use of relatively thick (380 µm) wafers and the moderately high bulk dopant concentration, as well as the lack of any active features to prevent rear side recombination (such as a back surface field or carrier selective contact).

It must be noted that, like almost all other reports of carbon nanotube–silicon heterojunction solar cells, the excellent initial performance was not stable and decreased over several hours or days before stabilizing at lower values. In the case of the copper doped solar cells, the efficiency decreased gradually over 3 d before stabilizing at ≈10–10.5% (Figure S8, Supporting Information) while, in the case of the polymer doped devices, the efficiency at first decreased rapidly in the first few hours, then more slowly over subsequent days, reaching ≈14–14.5% after one week (Figure S9, Supporting Information). For the copper colloid doping this was much worse than previous reports of long-term stability up to a year without any loss of performance.[7b] However, we highlight the fact that, compared to previous reports in which the copper colloid formed a thin contiguous layer on the cell surface, in our case the mildly hygroscopic colloid was present in the form of small crystallites that were exposed to the environment from all sides. In the case of the Nafion doping, since the doping effect has been previously shown to be stable,[14] we surmise that the initially rapid decrease in performance can be attributed to dehydration and thus deprotonation of the polymer, which has been previously shown to cause a steep decrease in passivation quality,[15] but highlight the fact that more work needs to be done in this area to draw any stronger conclusions. In both the copper colloid and Nafion doped devices, the likelihood of additional effects due to residual superacid in the nanotube film also cannot be ignored.

The devices were scaled up further to active areas of 5 cm^2 (2 cm × 2.5 cm) with a similar structure, but with wider contact fingers to account for the increased current and longer distance to the active area edge. However, the gold thickness was kept fixed at 300 nm (the same as for the 1 cm^2 devices, to avoid introducing potentially impactful differences at the edge of the active area where the nanotube films bridge the metal-oxide–silicon step structure) which meant that even with optimization of the finger width and pitch, the resistive power losses were higher (as evidenced by the lower fill factor and V_{OC}), to which we attribute the lower maximum efficiency of 15.5%

compared to the 1 cm² devices (Figure S10, Supporting Information). Nevertheless, these are still excellent results and are by far the largest such devices reported to date. Although these research grade devices are still based on the design of a front metal electrode framing the active area, rather than full surface devices with fingers and busbar(s), the use of 300 nm thick gold contacts precluded any enhancement of the performance due to current contributions which can come from outside of the framed area when light passes through much thinner metal layers (see Figure S11 and further discussion in the Supporting Information).

The state of the art in nanotube–silicon heterojunction solar cell design was combined with the outstanding carbon nanotube doping, surface antireflection, and silicon passivation properties of Nafion polymer to yield breakthrough performance from large area research grade devices. Although the Nafion polymer doping is not currently stable, it presents a new paradigm within the nanotube–silicon heterojunction architecture which could also be applied more broadly to other nanocarbon–semiconductor interfaces, and the challenge is now on to more fully understand the effects that have been described here, as well as to design or discover new functional analogues of this material with longer term stability. The reporting of high efficiency devices much larger than the key 1 cm² level further cements the potential of the carbon nanotube–silicon design and opens the way to the next level of full industrial wafer scale processing of this technology. Although it was not investigated in this work, it is likely that differences in contact resistance arising as a result of differences in contact fraction between nanotube/Nafion–silicon and nanotube/copper–silicon played a role in the measured differences in solar cell performance, and this should be investigated further. A potential method of resolving this and other issues related to contact between the nanotube film and the pyramid textured silicon, as well as improving the lifetime and contact/series resistance, could lie in the pyramid rounding technique, such as described by Ma et al.[19] To develop the carbon nanotube–silicon architecture further, major avenues for future work include using thinner silicon, full surface contact designs (rather than frames), and improved methods to reduce rear recombination through, for example, rear totally diffused contacts. Since the nanotube films always exhibit some degree of parasitic absorption when used as front side contacts, a further avenue could be to employ them instead on the back side of mono- or bifacial cells, where such absorption would be either irrelevant, or have only a negligible effect on the overall power output.

Supporting Information

Supporting Information is available from the Wiley Online Library or from the author.

Conflict of Interest

The authors declare no conflict of interest.

[1] a) D. D. Tune, B. S. Flavel, R. Krupke, J. G. Shapter, *Adv. Energy Mater.* **2012**, *2*, 1043; b) X. Li, Z. Lv, H. Zhu, *Adv. Mater.* **2015**, *27*, 6549; c) A. Di Bartolomeo, *Phys. Rep.* **2016**, *606*, 1; d) D. D. Tune, B. S. Flavel, *Adv. Energy Mater.* **2018**, *8*, 1703241; e) K. Huang, X. Yu, J. Cong, D. Yang, *Adv. Mater. Interfaces* **2018**, *5*, 1801520; f) K. Cui, S. Maruyama, *Prog. Energy Combust. Sci.* **2019**, *70*, 1; g) X. Kong, L. Zhang, B. Liu, H. Gao, Y. Zhang, H. Yan, X. Song, *RSC Adv.* **2019**, *9*, 863.

[2] a) J. Wei, Y. Jia, Q. Shu, Z. Gu, K. Wang, D. Zhuang, G. Zhang, Z. Wang, J. Luo, A. Cao, D. Wu, *Nano Lett.* **2007**, *7*, 2317; b) Y. Jia, J. Wei, K. Wang, A. Cao, Q. Shu, X. Gui, Y. Zhu, D. Zhuang, G. Zhang, B. Ma, L. Wang, W. Liu, Z. Wang, J. Luo, D. Wu, *Adv. Mater.* **2008**, *20*, 4594.

[3] a) Y. Jia, P. Li, J. Wei, A. Cao, K. Wang, C. Li, D. Zhuang, H. Zhu, D. Wu, *Mater. Res. Bull.* **2010**, *45*, 1401; b) K. Cui, T. Chiba, S. Omiya, T. Thurakitseree, P. Zhao, S. Fujii, H. Kataura, E. Einarsson, S. Chiashi, S. Maruyama, *J. Phys. Chem. Lett.* **2013**, *4*, 2571; c) K. Cui, A. S. Anisimov, T. Chiba, S. Fujii, H. Kataura, A. G. Nasibulin, S. Chiashi, E. I. Kauppinen, S. Maruyama, *J. Mater. Chem. A* **2014**, *2*, 11311; d) D. D. Tune, A. J. Blanch, R. Krupke, B. S. Flavel, J. G. Shapter, *Phys. Status Solidi A* **2014**, *211*, 1479.

[4] a) Y. Jia, A. Cao, F. Kang, P. Li, X. Gui, L. Zhang, E. Shi, J. Wei, K. Wang, H. Zhu, D. Wu, *Phys. Chem. Chem. Phys.* **2012**, *14*, 8391; b) C. Pintossi, G. Salvinelli, G. Drera, S. Pagliara, L. Sangaletti, S. D. Gobbo, M. Morbidoni, M. Scarselli, M. De Crescenzi, P. Castrucci, *J. Phys. Chem. C* **2013**, *117*, 18688; c) S. Ponzoni, G. Galimberti, L. Sangaletti, P. Castrucci, S. Del Gobbo, M. Morbidoni, M. Scarselli, S. Pagliara, *J. Phys. Chem. C* **2014**, *118*, 24110; d) C. Pintossi, S. Pagliara, G. Drera, F. De Nicola, P. Castrucci, M. De Crescenzi, M. Crivellari, M. Boscardin, L. Sangaletti, *ACS Appl. Mater. Interfaces* **2015**, *7*, 9436; e) S. Ponzoni, S. Achilli, C. Pintossi, G. Drera, L. Sangaletti, P. Castrucci, M. De Crescenzi, S. Pagliara, *ACS Appl. Mater. Interfaces* **2017**, *9*, 16627; f) D. D. Tune, H. Shirae, V. Lami, R. J. Headrick, M. Pasquali, Y. Vaynzof, S. Noda, E. K. Hobbie, B. S. Flavel, *ACS Appl. Energy Mater.* **2019**, *2*, 5925.

[5] a) P. Wadhwa, G. Seol, M. K. Petterson, J. Guo, A. G. Rinzler, *Nano Lett.* **2011**, *11*, 2419; b) P. Wadhwa, B. Liu, M. A. McCarthy, Z. Wu, A. G. Rinzler, *Nano Lett.* **2010**, *10*, 5001; c) Y. Jung, X. Li, N. K. Rajan, A. D. Taylor, M. A. Reed, *Nano Lett.* **2013**, *13*, 95; d) D. D. Tune, F. Hennrich, S. Dehm, M. F. G. Klein, K. Glaser, A. Colsmann, J. G. Shapter, U. Lemmer, M. M. Kappes, R. Krupke, B. S. Flavel, *Adv. Energy Mater.* **2013**, *3*, 1091; e) J. M. Harris, R. J. Headrick, M. R. Semler, J. A. Fagan, M. Pasquali, E. K. Hobbie, *Nanoscale* **2016**, *8*, 7969.

[6] F. Wang, D. Kozawa, Y. Miyauchi, K. Hiraoka, S. Mouri, Y. Ohno, K. Matsuda, *Nat. Commun.* **2015**, *6*, 6305.

[7] a) E. Shi, L. Zhang, Z. Li, P. Li, Y. Shang, Y. Jia, J. Wei, K. Wang, H. Zhu, D. Wu, S. Zhang, A. Cao, *Sci. Rep.* **2012**, *2*, 884; b) K. Cui, Y. Qian, I. Jeon, A. Anisimov, Y. Matsuo, E. I. Kauppinen,

S. Maruyama, *Adv. Energy Mater.* **2017**, *7*, 1700449; c) H. Wu, X. Zhao, Y. Sun, L. Yang, M. Zou, H. Zhang, Y. Wu, L. Dai, Y. Shang, A. Cao, *Sol. RRL* **2019**, *3*, 1900147.

[8] a) X. Li, Y. Jung, J.-S. Huang, T. Goh, A. D. Taylor, *Adv. Energy Mater.* **2014**, *4*, n/a; b) W. Xu, S. Wu, X. Li, M. Zou, L. Yang, Z. Zhang, J. Wei, S. Hu, Y. Li, A. Cao, *Adv. Energy Mater.* **2016**, *6*, 1600095; c) L. Yu, T. Grace, M. D. Jazi, C. Shearer, J. Shapter, *Sol. RRL* **2017**, *1*, 1600026.

[9] Y. Jia, A. Cao, X. Bai, Z. Li, L. Zhang, N. Guo, J. Wei, K. Wang, H. Zhu, D. Wu, P. M. Ajayan, *Nano Lett.* **2011**, *11*, 1901.

[10] X. Li, L. M. Guard, J. Jiang, K. Sakimoto, J.-S. Huang, J. Wu, J. Li, L. Yu, R. Pokhrel, G. W. Brudvig, S. Ismail-Beigi, N. Hazari, A. D. Taylor, *Nano Lett.* **2014**, *14*, 3388.

[11] a) D. D. Tune, B. S. Flavel, J. S. Quinton, A. V. Ellis, J. G. Shapter, *ChemSusChem* **2013**, *6*, 320; b) L. Yu, D. D. Tune, C. J. Shearer, J. G. Shapter, *ChemNanoMat* **2015**, *1*, 115; c) L. Yu, M. Batmunkh, T. Grace, M. Dadkhah, C. Shearer, J. Shapter, *J. Mater. Chem. A* **2017**, *5*, 8624.

[12] L. Yu, D. D. Tune, C. J. Shearer, J. G. Shapter, *Sol. Energy* **2015**, *118*, 592.

[13] a) E. Muramoto, Y. Yamasaki, F. Wang, K. Hasegawa, K. Matsuda, S. Noda, *RSC Adv.* **2016**, *6*, 93575; b) L. Yu, M. Batmunkh, M. Dadkhah, C. J. Shearer, J. G. Shapter, *Energy Environ. Mater.* **2018**, *1*, 232.

[14] I. Jeon, C. Delacou, H. Okada, G. E. Morse, T.-H. Han, Y. Sato, A. Anisimov, K. Suenaga, E. I. Kauppinen, S. Maruyama, Y. Matsuo, *J. Mater. Chem. A* **2018**, *6*, 14553.

[15] J. Chen, K. Ge, C. Zhang, J. Guo, L. Yang, D. Song, F. Li, Z. Xu, Y. Xu, Y. Mai, *ACS Appl. Mater. Interfaces* **2018**, *10*, 44890.

[16] R. Li, J. Di, Z. Yong, B. Sun, Q. Li, *J. Mater. Chem. A* **2014**, *2*, 4140.

[17] Using a version of the Java applet "Optimisation of finger spacing" from http://www.pveducation.org, modified to allow Finger Depths of <1 micron.

[18] X. Li, Y. Jung, K. Sakimoto, T.-H. Goh, M. A. Reed, A. D. Taylor, *Energy Environ. Sci.* **2013**, *6*, 879.

[19] K. Ma, X. Zeng, Q. Lei, J. Xue, Y. Wang, C. Zhao, *Front. Optoelectron.* **2014**, *7*, 46.